NASA
Technical
Paper
2486

June 1985

Fluid Surface Behavior in Low Gravity

Center Discretionary Fund No. 83-21, Final Report

Fred Leslie,
Roger F. Gans,
and Charles Schafer

NASA

NASA Technical Paper 2486

1985

Fluid Surface Behavior in Low Gravity

Center Discretionary Fund No. 83–21, Final Report

Fred Leslie,
Roger F. Gans,
and Charles Schafer

George C. Marshall Space Flight Center
Marshall Space Flight Center, Alabama

NASA

National Aeronautics and Space Administration

Scientific and Technical Information Branch

ACKNOWLEDGMENTS

The authors would like to thank Robert Shurney for his help in coordinating the aircraft activities. This work was supported by the Marshall Space Flight Center Discretionary Fund No. 83-21.

TABLE OF CONTENTS

LIST OF ILLUSTRATIONS

NOMENCLATURE

C	constant of integration
$f(r)$	height of interface
F	rotational Bond number
g	gravitational acceleration
G	Bond number
L	container half depth
$\hat{n}_o$	unit normal outward-pointing vector
p^i	pressure inside bubble
p^o	pressure outside bubble
$p_o{}^i, p_o{}^o$	pressure constants
p_o	pressure difference = $p_o{}^i - p_o{}^o$
r	radial coordinate
$\hat{r}$	nondimensional radial coordinate
r_o	radius of interface contact with boundary
$\hat{r}_o$	nondimensional radius of interface contact with boundary
R	maximum bubble radius
T	coefficient of surface tension
y	nondimensional capillary rise
z	vertical coordinate
$\hat{z}$	nondimensional vertical coordinate
z^B	distance from bubble equator to container bottom
z^T	distance from bubble equator to container top
Δ	total radius of curvature
ζ	capillary rise

θ	contact angle
ρ_i	density of fluid inside bubble
ρ_o	density of fluid outside bubble
ρ	density difference = $\rho_i - \rho_o$
ϕ	slope of interface = df/dr
ψ	integration parameter
ω	rotation rate

TECHNICAL PAPER

FLUID SURFACE BEHAVIOR IN LOW GRAVITY

Center Discretionary Fund No. 83-21, Final Report

INTRODUCTION

Free surface shapes of liquids play a key role in spacecraft fuel tank design and fluid management systems. In the absence of gravity and temperature gradients along the surface, which drive Maragoni convection, the equilibrium shape of the free surface is governed by a balance of capillary and centrifugal forces. Hydrostatic stability is maintained when the additional pressure from the capillary rise is compensated for by the pressure reduction due to the curvature of the free surface. In a zero gravity environment without rotation, the surface is spherical. As to whether the sphere encloses the liquid or the vapor depends on the wetabilty of the container by the liquid. In some spacecraft fuel tank applications, propellant slosh and distribution are controlled with the use of internal baffles which come into contact with the free surface. If the liquid is to be held using capillary forces, the baffle spacing must be small enough to overcome the fluid's inertial forces during small accelerations brought about by thruster firings, crew motion, etc. The problem can be complicated by the rotation of the container. In any case, in order to manage the liquid, the distribution of the fluid including its interface shape must be determined.

Rosenthal [1] computed the shapes of rotating bubbles in the absence of gravity. He found that for large rotation rates, the aspect ratio of a free bubble is proportional to the square of the rotation rate. Chandrasekhar [2] examined the stability of a rotating liquid drop in which he derived analytical formulas for the equilibrium shapes based on Laplace's equation for the pressure drop across the interface. He went on to determine the frequency of the oscillations for various modes. Busse [3] also examined the frequency of small oscillations for drops and bubbles. Using a spherical coordinate system, he determined the equilibrium shape for a rotating liquid drop in terms of a Legendre function expansion. He determined that for drops, the frequency of oscillation increases with rotation rate. The opposite result occurs for bubbles. Tieu, et al. [4] obtained solutions for the motion and interface shape of a two-fluid system contained in an oscillating vertical cylinder. Using a domain perturbation approach, they obtained first and second order solutions in a one-g environment. Experimental results were in qualitative agreement with their theoretical predictions.

Princen, et al. [5] measured interface shape characteristics of bubbles. However, in order to perform the experiments in a one-g environment, the rotation rate had to be high enough for centrifugal forces to be much greater than gravitational forces. Consequently, the bubble interfaces were shaped like cylinders with round ends. Gans [6] obtained numerical solutions for rotating bubbles enclosed in baffled containers and found that gravity had a destabilizing influence on their position. The solutions were validated experimentally in a one-g environment. Experiments with non-axisymmetric shapes of a rotating drop immersed in a host medium were performed by Wang, et al. [7]. They observed a family of multilobe shapes as a function of a rotational Bond number. Experimental results have also been obtained by acoustic excitation of drops (Trinh, et al. [8]).

The Fluid Interface and Bubble Experiment (FIBEX) was conceived and developed in order to answer questions concerning low-gravity fluid behavior which were raised by design and operational considerations for the Gravity Probe-B (GP-B) experiment. Early phases of GP-B design studies have been carried out at the Marshall Space Flight Center (MSFC) and at Stanford University. The GP-B

experiment is aimed at testing aspects of general relativity theory predicting precession of an orbiting gyroscope due to interactions with the Earth's gravitational field. A concept for the GP-B design which is the result of MSFC studies is shown in Figure 1. The gyroscope package is surrounded by a large liquid helium dewar and spacecraft power and control systems. A design goal for the system is that over the one-year lifetime of the experiment, accelerations at the gyro locations be kept at 10^{-10} g or below. The liquid helium dewar depletes itself over this period by providing cooling and propulsive venting for the attitude and drag-free control systems. This action creates significant excursions in the total mass of the satellite. This mass change is not a problem if the liquid helium distribution remains symmetric about the spacecraft center of mass. If large deviations from symmetry occur, then gravitational and gravity gradient effects can produce significant degradation of experiment performance. It has been shown (Schafer, et al. [9]) that for worst case liquid helium configurations, accelerations at the experiment location could be one or two orders of magnitude greater than the upper design limit. It was also shown that the dominant forces for determining the fluid distribution are surface tension and centrifugal force, which for GP-B are of the same magnitude. In this regime, the liquid helium configuration is not readily predictable, but a symmetric distribution appears unlikely.

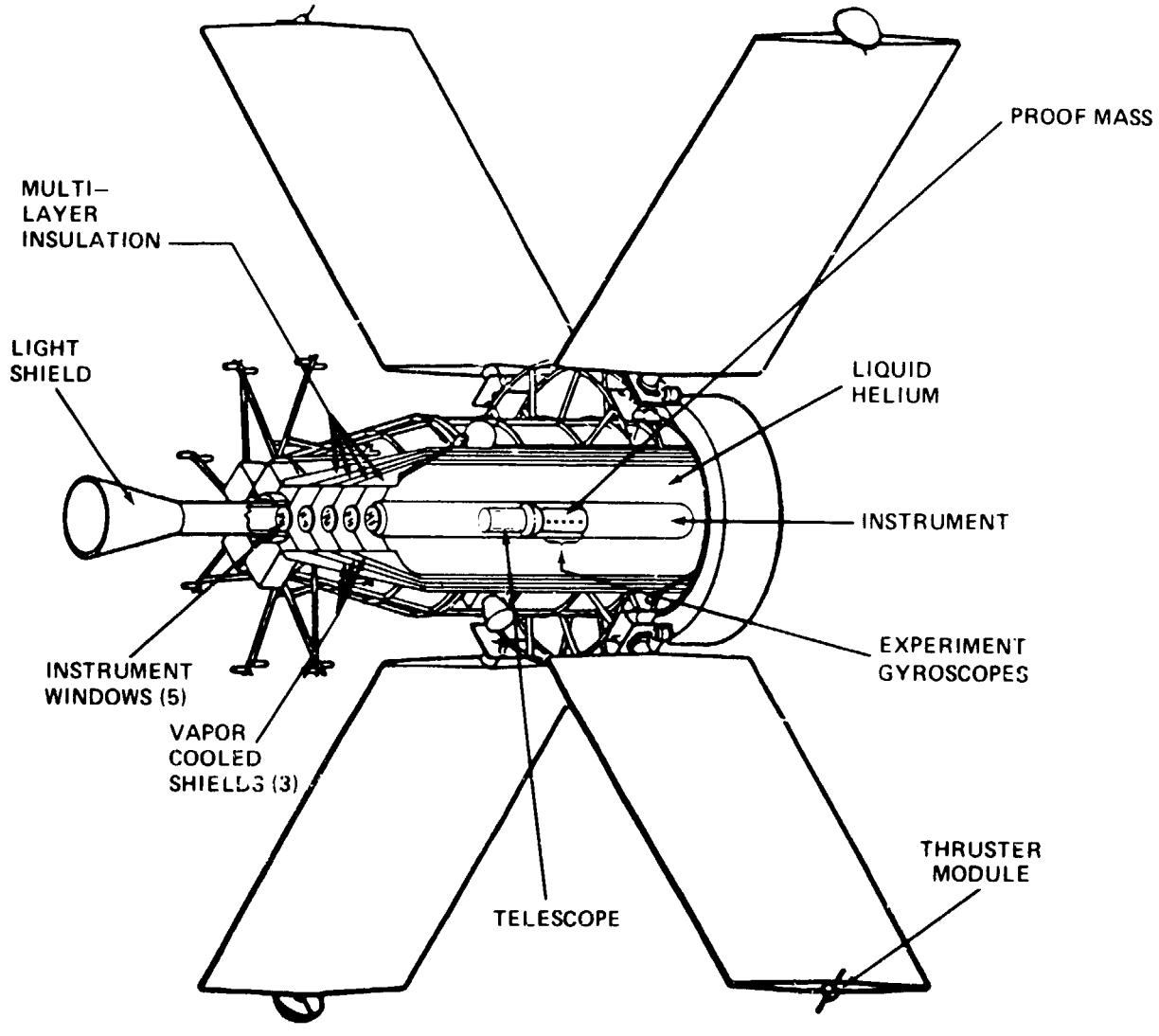

Figure 1. Gravity Probe-B conceptual design.

Based on these considerations, an approach was suggested which was aimed at achieving a symmetrical liquid helium distribution and maintaining it during the experimental period. This approach involved installation of a set of baffle plates in the liquid helium dewar, as shown in Figure 2 The higher spin rates planned for initiation of the experiment are sufficient to cause centrifugal forces to dominate surface tension and drive the fluid into an axisymmetric shape. Submerged slots were introduced in order to allow the fluid to transfer more easily. When the spin rate is reduced to the operational level, the baffles would hold the fluid in place through capillary forces.

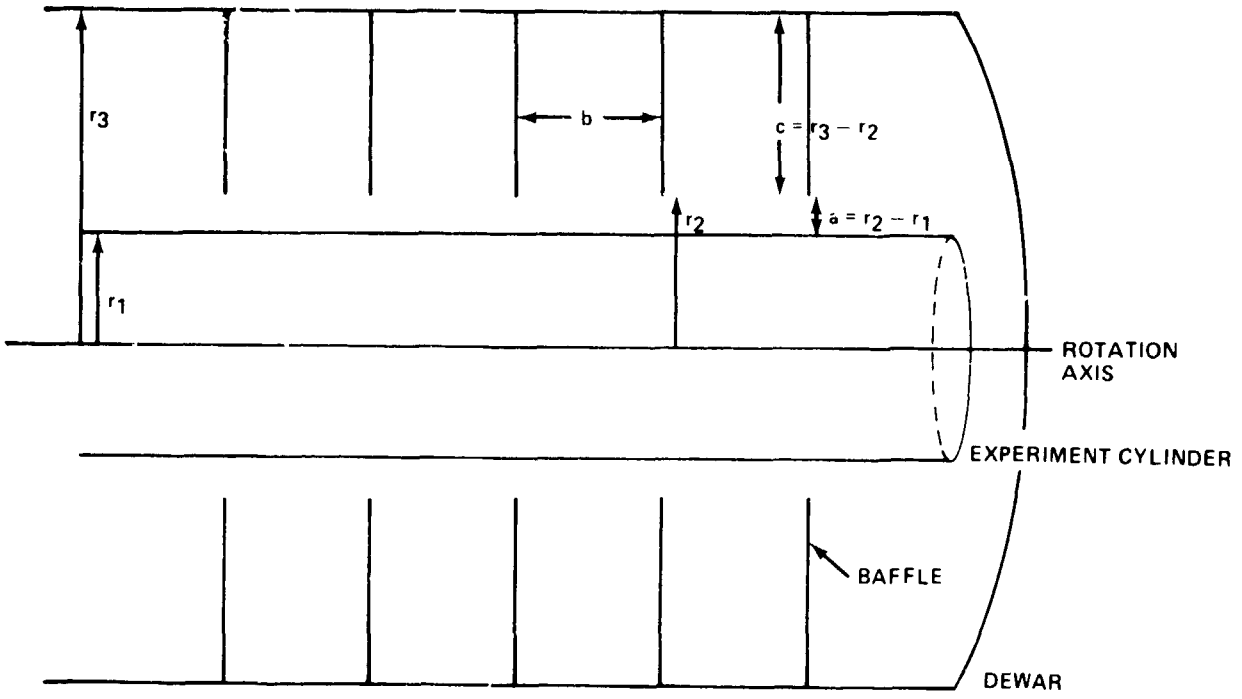

Figure 2. Liquid helium dewar with baffles.

Given that the desired liquid helium configuration can be achieved, the question of shape stability arises. Results of a static stability analysis are presented in this paper. It will be shown that two types of instability are possible. The first type results from the baffle spacing being so wide that the surface of the liquid between the baffles cannot form a meniscus, i.e., the surface would "roll up." The second type of instability possible results from adjacent fluid cells communicating with each other through the submerged slots. Displacement of one fluid level away from the axis forces an adjacent level toward the axis. In certain regions of parameter space, the additional hydrostatic pressure attained by the latter level is not enough to compensate for the deficit resulting from the smaller radius of curvature. Consequently, the displacement is enhanced.

Although this work was initially motivated by the GP-B fluid management problem, a more general study has been performed which examines the physical processes which govern the behavior of rotating free surfaces in a low-gravity environment. A laboratory investigation of the phenomena requires that centrifugal force be much greater than gravity, a condition that can be achieved in a terrestrial laboratory by rotating the fluid at high rates. However, it is also required that surface tension forces be as important as centrifugal forces, a condition that could not be attained unless length scales were made exceedingly small. This not only makes observations difficult, but also introduces viscous effects by greatly reducing the Reynolds number. In this paper, measurements of rotating equilibrium free surface shapes in the low-gravity environment of a free-falling aircraft are presented. This allows varying the relative importance of surface tension with respect to centrifugal forces producing a variety

of shapes for comparison with theoretical profiles. Calculations of the shapes are made using a more general formulation of Chandrasekhar's equation by including contact of the interface with the rotating container at a specified angle. It is easily shown that an isolated bubble or drop is a special case of the general result.

INTERFACE EQUATION

Figure 3 shows a cross-section of a partially-filled cylindrical container rotating about the vertical axis. The fluid is centrifuged against the outer wall and forms a meniscus which intersects the horizontal boundaries at an angle θ. The horizontal baffles are separated by a spacing 2L. The distance from the axis of rotation to the farthest point along the vapor/liquid interface is given by R and the capillary rise with respect to this point is given by $\zeta(z)$. The fluid interface intersects the top of the cylinder at a height of z^T and at the bottom at z^B. The pressure inside the bubble p^i is given by

$$p^i = p_o{}^i + \frac{1}{2} \rho_i \omega^2 r^2 - \rho_i g z \tag{1}$$

where $p_o{}^i$ is a constant, ρ_i is the density of the fluid inside the interface and ω is the rotation rate of the fluid. The pressure outside of the bubble p^o is given by

$$p^o = p_o{}^o + \frac{1}{2} \rho_o \omega^2 r^2 - \rho_o g z \tag{2}$$

where $p_o{}^o$ is a constant, and ρ_o is the density of the fluid outside the interface. At the interface, the pressure discontinuity is given by LaPlace's formula

$$p^i - p^o = T \nabla \cdot \hat{n}_o \tag{3}$$

where T is the coefficient of surface tension and $\hat{n}_o$ is the unit normal pointing outward from the surface. Let the position of the interface be given by $r = R - \zeta(z)$. Then the right hand side of equation (3) is

$$\frac{1}{r\Delta} + \frac{1}{\Delta^3} \frac{d^2\zeta}{dz^2}$$

where

$$\Delta = \left[1 + \left(\frac{d\zeta}{dz}\right)^2\right]^{1/2}$$

Substituting equation (1) and equation (2) into equation (3) along with nondimensionalizing r and z with R, the general equation for the interface becomes

$$1 + y_o'' = 8Fy(y/2 - 1) - G\,\hat{z} + (1 + y'^2)^{-1/2}\left[\frac{1}{1-y} + \frac{y''}{1+y'^2}\right]$$

where y_o'' is the nondimensional curvature at the point R, y is the nondimensional capillary rise and F and G are the parameters which determine the interface shape given by

$$F = \frac{(\rho_o - \rho_i)\,\omega^2\,R^3}{8T}$$

and

$$G = \frac{(\rho_o - \rho_i)\,g\,R^2}{T}$$

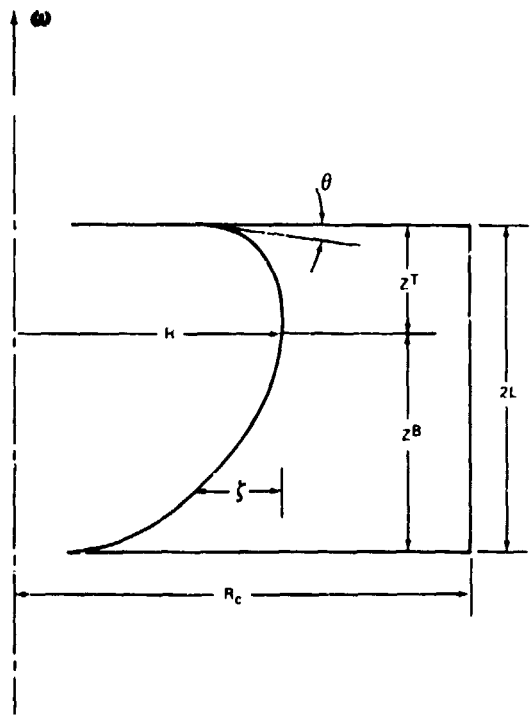

Figure 3. Definition sketch of the cylindrical coordinate system used for the analytical model.

The parameter F represents the ratio of centrifugal force to surface tension while G is a ratio of gravitational force to surface tension. Note that F is negative for rotating drops ($\rho_i > \rho_o$) and positive for rotating bubbles ($\rho_i < \rho_o$). Of course for large F and G, the classic parabolic interface shape is obtained. In that case, the equation reduces to

$$8\,Fy\left(\frac{1}{2}\,y - 1\right) = G\,\hat{z} \quad .$$

Recalling that $y = \zeta/R$, $\hat{z} = z/R$ and the radial position of the interface is $r = R - \zeta$, solving for z gives

$$z = \frac{\omega^2}{2g}\,(r^2 - R^2) \quad .$$

The general interface equation is solved using a fourth order Runge-Kutta scheme with a stretched interval. The integration is performed, for a given F, by starting at z = 0 with a guess for y_o'' and integrating first in the forward direction until the boundary condition (contact angle) is met and then starting again at z = 0 and integrating in the negative direction.

For space applications, calculations were made for small F and for zero G. These results are shown in Figure 4 with the maximum nondimensional baffle spacing (2L/R=D) as a function of F. The curve indicates the maximum baffle spacing necessary to have an interface which intersects both the top and bottom baffle. For baffle spacings below the curve, the fluid configuration is considered stable since the interface has been captured by the baffles and its position and shape are known. For conditions above the curve, at least one baffle is not in contact with an interface implying that a bubble has formed whose position is unknown. This is referred to as a type I instability.

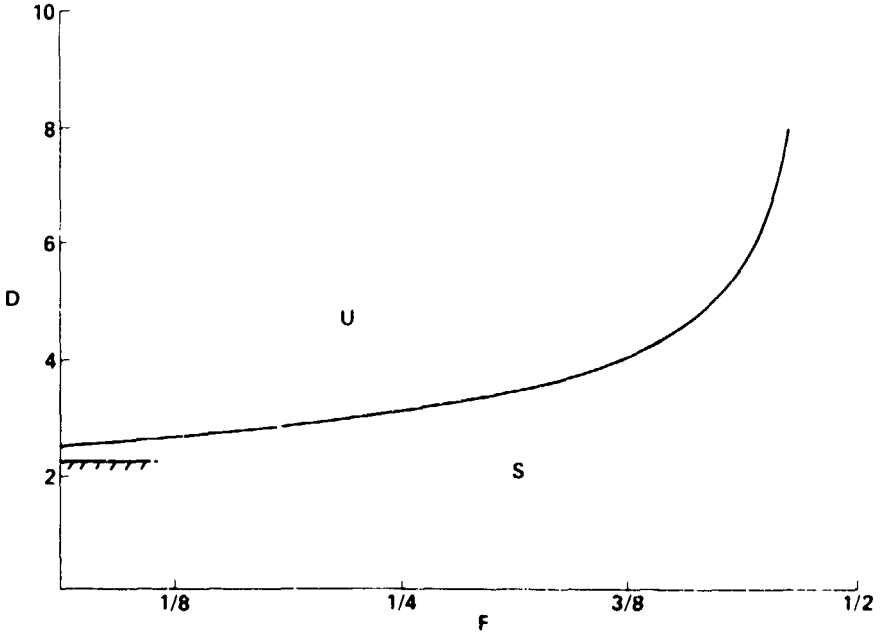

Figure 4. Neutral stability curves for zero gravity.

Solutions to the interface equation also indicated a second type of instability relevant to adjacent baffles open at the bottom to allow fluid interchange. Consider Figure 5, which shows two adjacent and equal columns. For large F, the downward displacement of one column would produce a rise in the other. The higher column would produce a larger hydrostatic pressure at the port level and force fluid back through, returning the free surfaces to their original equal levels. However, for very small values of F the rising column would continue to rise because its pressure at the port has been reduced more by the greater surface tension (smaller radius of curvature) than it has been increased by hydrostatic pressure. The important consideration is how the pressure difference across the baffle varies with R during perturbations. Solutions to the interface equation (with G=0) were used to obtain this information and the results are shown in Figure 6 along with the curve of Figure 4 for comparison. Obviously, this phenomenon places a more strict baffle spacing requirement through setting a surface tension length scale which dominates the radial one.

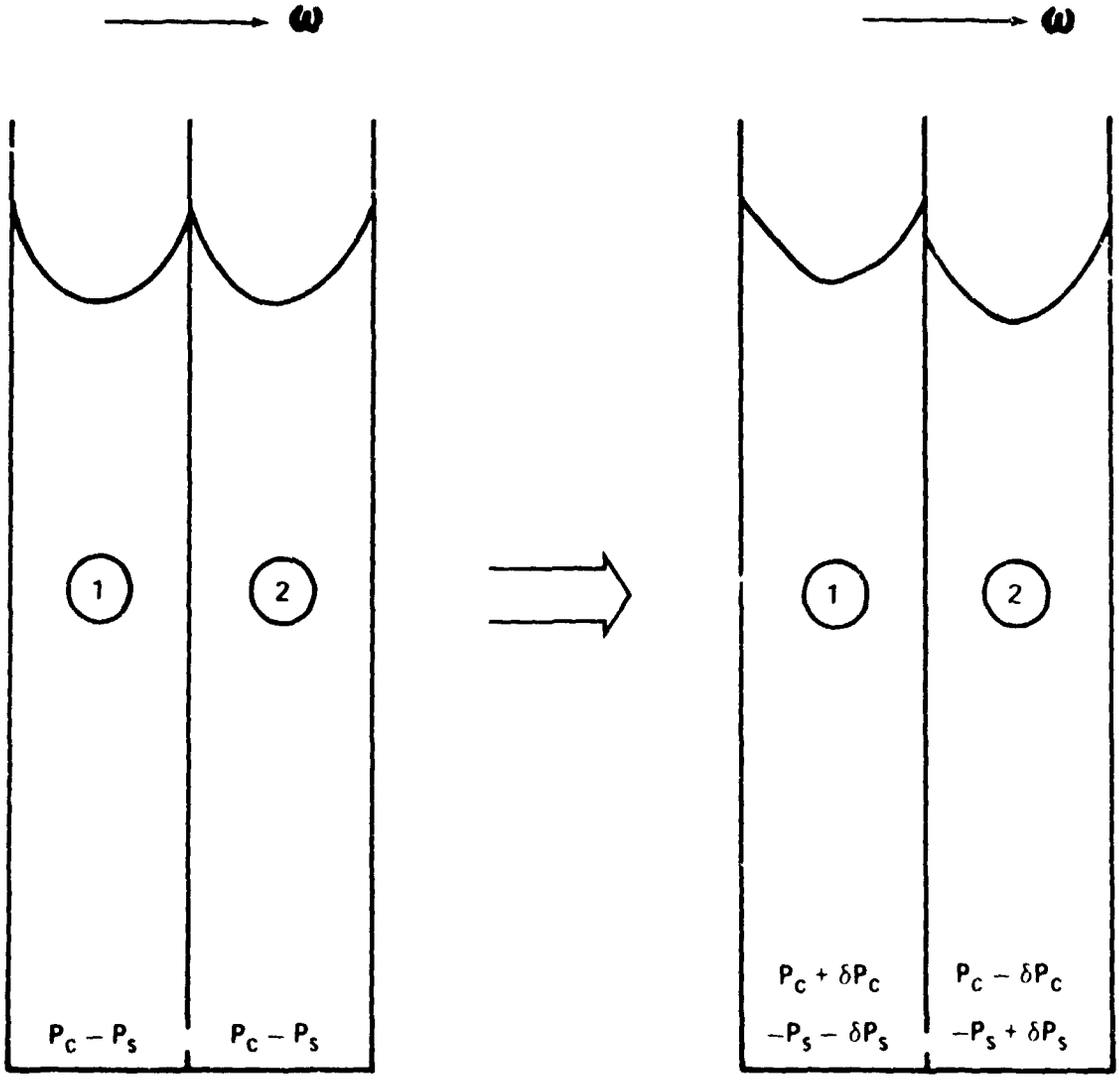

Figure 5. Sketch of the type II instability phenomenon.

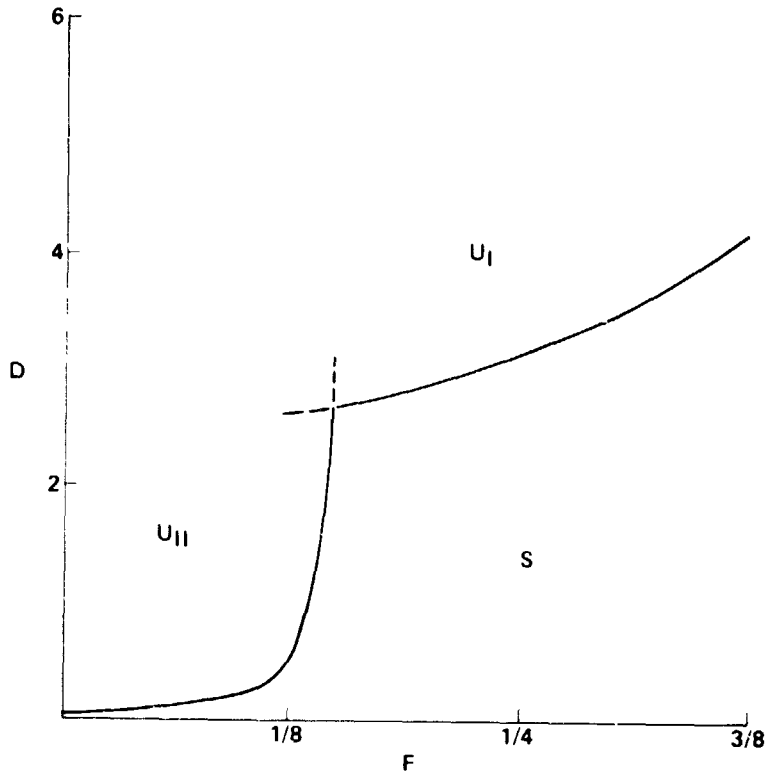

Figure 6. Type II neutral stability curves for zero gravity along with curve from Figure 4.

GROUND-BASED EXPERIMENTS

One motivation for adding gravity to the analysis in the previous section was the hope that useful experiments could be done in the laboratory. Ideally, one would want small G and moderate F to attempt to model space applications. That proves to be impractical for reasonable values of R and ω. If ρ, g, and T are fixed, then

$$R = [GT/\rho g]^{1/2}$$

and

$$\omega = [8TF/\rho R^3]^{1/2}$$

and, to use ethanol as an exemplary fluid, if G = 0.1 and F = 1, then R = 0.16 mm and ω = 6800/sec.

While a model experiment is impossible, it seemed useful to explore the basic premises of the model in a ground-based laboratory before proceeding to a low-gravity environment. To that end a set of experiments in a shallow dish were performed. All that could be observed easily was the location of

the top interface (where the liquid intersects the upper boundary) and whether the liquid intersects the lower boundary. If 2L exceeds the maximum value for a given F, the liquid will intersect only the top surface.

The experiments were carried out in a small petri dish (diameter = 48.06 mm, depth = 8.59 mm) mounted to a turntable. Centering accuracy was better than 0.8 mm. Turntable speed was accurate to better than 5 parts per thousand in the range of interest. The working fluid was ethanol colored with India ink at 2 drops for 25 ml ethanol. A contact angle of zero was assumed.

The measured dependent variable was the apparent intersection radius of the fluid with the upper boundary as a function of rotation rate and air volume. The observation was made visually by watching the position of the intersection against a marked upper surface grid. Errors arising from non-concentricity and parallax are estimated to be 0.5 mm. There is an additional systematic error which may lead one to overestimate the radius. This arises because the visible intersection line is not the true intersection line, but is some point at which the coloring is dark enough to see. The nearer the contact angle is to zero, the more pronounced this effect will be.

Results are shown in Figure 7 for air volumes of 2, 4, and 6 ml. The symbols denote data and the solid lines joining open circles are calculated results. The calculation predicts bottom exposure for the 6 ml case at rotation rates above 18/sec, and the observations are consistent with the prediction. The four right-most symbols on the upper curve showed a clearly exposed bottom. The next two were ambiguous. All the others, on all the curves, showed the bottom covered.

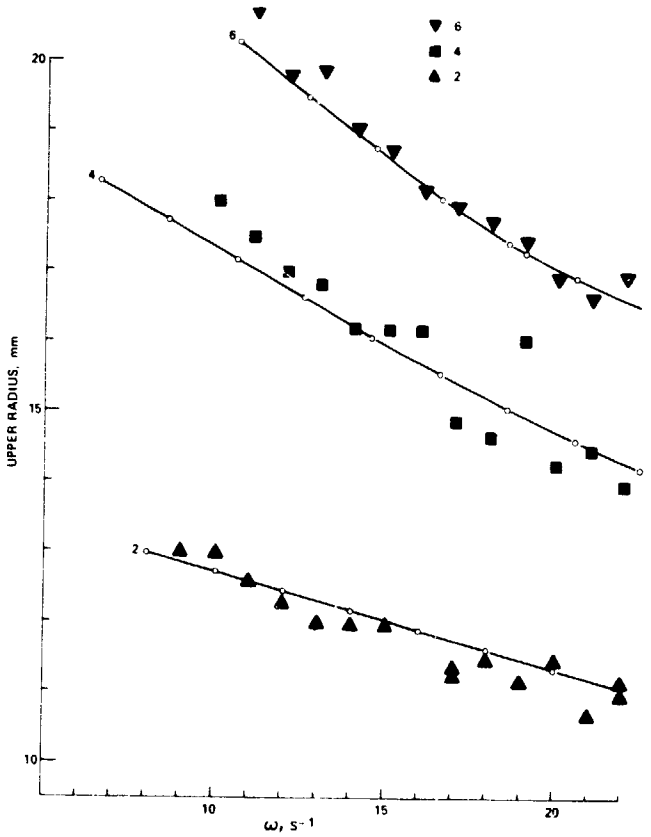

Figure 7. Ground-based measurements of the intersection of upper interface with the boundary versus rotation rate for various bubble volumes.

KC-135 EXPERIMENT PACKAGE

A schematic of the apparatus flown in the low-gravity environment of the KC-135 aircraft is shown in Figure 8. It consists of a test cell cylinder, a turntable assembly, and a photographic system. The test cell is made from acrylic and polycarbonate (Plexiglass and Tuffak, respectively). It measures 20 cm across while the depth can be set at 2 cm, 4 cm, or 6.3 cm. The cylinder is partially filled with ethanol, chosen because its surface tension is relatively high and not extremely sensitive to low levels of contamination, its contact line with the container does not stick, and its contact angle is close to zero. The cylinder is fastened to a turntable which rotates about the cylinder's axis. The turntable is mounted on a hollow shaft suspended by ball bearings. The electrical wiring, including a coaxial cable, are routed through the hollow shaft and external connections are made through a 16-contact slipring assembly. The turntable is 16 in. in diameter and has a centering pin for locating the test cell precisely coaxial with the rotation axis. A camera frame accommodates a video or cine camera above the test cell. The camera mount adjusts so that the viewing direction can be aligned with the rotation axis. The camera mount can be balanced for smooth rotation using a system of counterweights. Two adjustable, shielded light fixtures are mounted to the table columns and are covered with fine mesh screen to restrain glass fragments should the bulbs rupture. The turntable is driven by a gear motor through a timing belt and clutch mechanism. A speed controller permits adjustment of the turntable rotation speed. The rotation speed can be varied from 0 to 108 rpm. A tachometer measures the motor rotation rate and displays the information on an LED display. The motor and turntable assembly are mounted on a frame which can swivel about a horizontal axis. This permits maintenance of the turntable rotation axis alignment with a space-fixed axis as the KC-135 aircraft pitches. This entire fixture is mounted on a subassembly which is bolted to the floor of the aircraft. The fixture can be released from the subassembly for free-

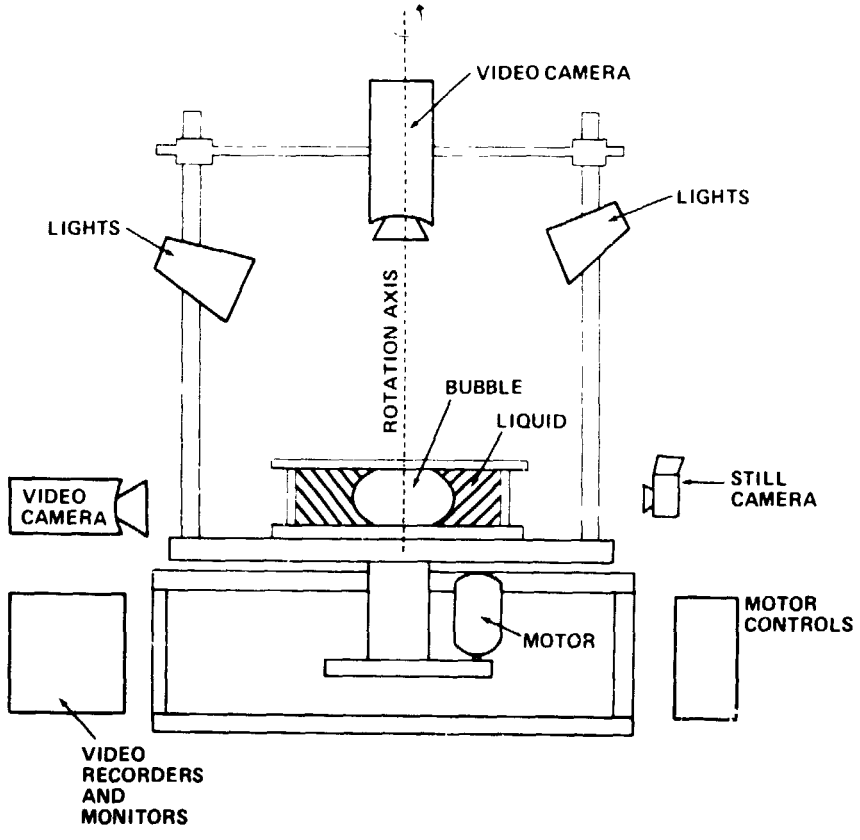

Figure 8. A schematic of the experimental apparatus.

floating the package to further reduce the acceleration levels. Power required by the experiment is 110 Vac. This drives the motor, lights, and video recorders. A dc power supply operates from the 110 Vac and provides 12 Vdc or 24 Vdc for use by the video or cine cameras. Operation of the experiment is performed via the control box. The main power supply switch is located here along with controls for the motor speed, lights, a turntable tachometer, and the camera power.

After the cylinder is filled with ethanol, a prescribed amount is removed to establish the bubble volume. Overhead and side-mounted video and still cameras record the shape of the fluid interface. The video cameras were particularly useful. The focus, field of view, and lighting could be instantly evaluated by observing the video monitor. In addition, immediate playback was possible to insure that a particular phenomenon was captured. The audio tracks on the tape also allowed for voice annotation. The 16 mm camera was less versatile and sometimes had poor exposures from the varying light levels in the aircraft cabin. Use of this camera was later abandoned.

The apparatus was bolted to the floor of a KC-135 aircraft which is flown in a parabolic trajectory that provides 20 to 30 sec of low gravity. Figure 9 shows a typical trajectory. After a descent from about 35,000 ft to 25,000 ft the aircraft attains an airspeed of 520 mph and then pitches sharply upward to begin the parabola. The local apparent gravity begins to diminish to near zero. Its value is measured by accelerometers. Although the gravity fluctuates around zero, typical departures are of the order of two percent of terrestrial gravity. At the top of the arc near 35,000 ft the airspeed has reduced to 320 mph and the aircraft pitches down for the second half of the parabola. The maneuver is completed when the aircraft has descended to 25,000 ft and another parabola begins. On several occasions the apparatus was free-floated in the cabin in an attempt to reduce the g levels as well as the fluctuations. However, because the package was so large, it often had to be grasped by personnel to prevent it from coming into contact with the aircraft walls or other experiments.

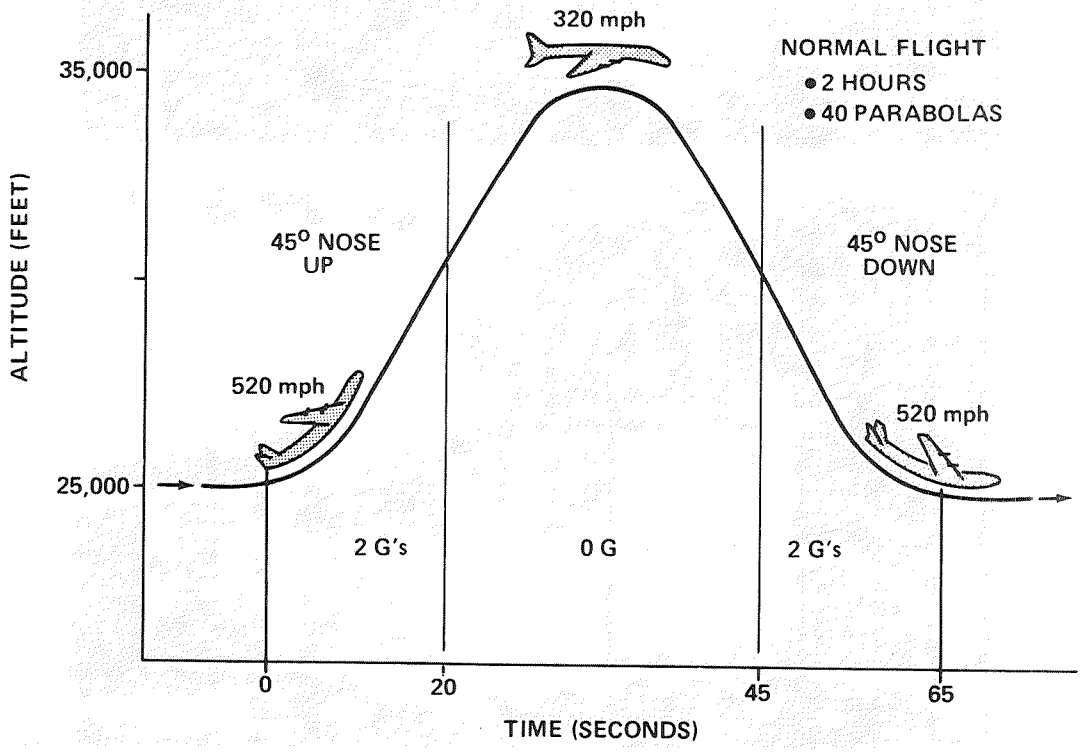

Figure 9. The parabolic trajectory flown by the KC-135 aircraft for the low gravity maneuver.

The fluid is set into rotation before the maneuver begins and the bubble shape is determined primarily by the centrifugal and gravitational forces, producing the classic paraboloidal surface. During the aircraft pullout at the start of the maneuver, the fluid experiences 2-g's which flattens the bubble at the top of the cylinder. As the local gravity diminishes the vapor penetrates down the axis of the cylinder. The interface appears as a miniscus symmetric about the axis. Figure 10 shows typical bubbles for (a) relatively strong rotation compared to surface tension, and (b) weak rotation. For the latter case, the bubbles tend to meander somewhat and their shape is more sensitive to fluctuations of the low-gravity environment. This is consistent with Rosenthal's analytical result that rotation has a stabilizing effect.

Analysis of the data is performed in four steps. First, a photographic frame of the bubble is digitized to provide coordinates for the liquid-vapor interface. Next, the shape is scaled to actual size using ratios of known dimensions. Then, the data is corrected for optical distortion using a ray trace algorithm. Finally, the volume of the bubble is computed from the coordinates of the interface and compared with the measured value.

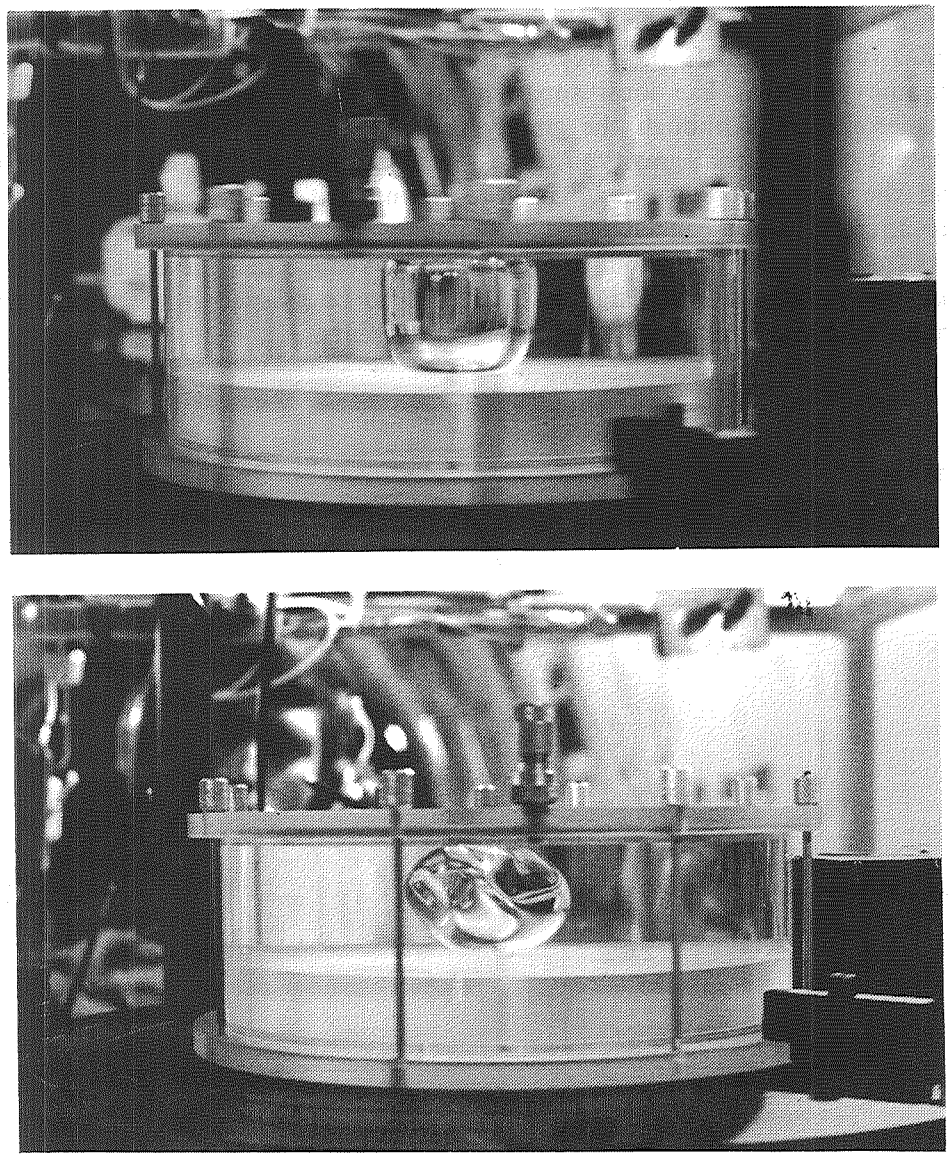

Figure 10. Typical shape for a bubble (a) dominated by centrifugal force and (b) dominated by surface tension.

ANALYTICAL MODEL OF FLIGHT EXPERIMENTS

The previous analysis is simplified for the case of G = 0 and a slightly different derivation simplifies the interface equation to one that is directly integrable. Chanrasekhar's [2] analysis is expanded to develop an equation for the interface shape relevant to the flight experiments. The bubble is assumed to be symmetric about the axis as well as its equator. The fluid interface intersects the top of the cylinder at a height of L and at a radius of r_o. For this case, let the position of the interface be given by z = f(r). Then the right hand side of equation (3) is

$$- T \frac{d}{dr} \frac{r\phi}{\sqrt{1 + \phi^2}}$$

where $\phi \equiv df/dr$. Again substituting equation (1) and equation (2) into equation (3), and making use of the above expression yields

$$p_o r + \frac{1}{2} \rho \omega^2 r^2 = - T \frac{d}{dr} \frac{r\phi}{\sqrt{1 + \phi^2}} \tag{4}$$

where $p_o = p_o^i - p_o^o$ and $\rho = \rho_i - \rho_o$. One integration of equation (4) results in

$$\frac{1}{2} p_o r^2 + \frac{1}{8} \rho \omega^2 r^4 = - \frac{T r \phi}{\sqrt{1 + \phi^2}} + C$$

where C is a constant. The value of C can be determined by the boundary condition that at $r = r_o$, $\phi = - \tan\theta$. The value of p_o can be evaluated at r = 0 where $\phi \to -\infty$. With these substitutions along with nondimensionalizing r and z with R, the general equation for the interface becomes

$$f(\hat{r}) = \int_1^{\hat{r}} \frac{\psi}{\sqrt{1 - \psi^2}} \, d\hat{r} \tag{5}$$

where

$$\psi = \frac{1 - \hat{r}_o \sin\theta + F (1 - \hat{r}_o^4)}{1 - \hat{r}_o^2} \frac{\hat{r}_o^2 - \hat{r}^2}{\hat{r}} + \frac{F (\hat{r}^4 - \hat{r}_o^4)}{\hat{r}} - \frac{\hat{r}_o \sin\theta}{\hat{r}}$$

and ^ denotes nondimensional radii. Note if $\hat{r}_o = 0$ and $\theta = 0$, equation (5) is equivalent to Chandrasekhar's equation for the shape of a rotating free drop. For the case F = 0, equation (5) represents a sphere. Chandrasekhar presented solutions for drops in which case $\hat{r}_o = 0$, $\theta = 0$, and F is negative. He showed that the boundary conditions for the equations could be met only for $F > -2.32911$. Otherwise, the rotation was strong enough to centrifuge all the liquid away from the axis forming a torus-like drop.

This investigation examines rotating bubbles which may intersect the top and bottom boundaries. In this case $F > 0$ and $\hat{r}_o$ may not be 0. It can be shown that there is a maximum value of F above which the bubble interface no longer contacts the axis. By taking the derivative of ψ with respect to $\hat{r}$ and setting it equal to zero, we can see that in the marginal case of $\hat{r}_o = 0$, ψ is a maximum at $\hat{r} = \sqrt{(1+F)/3F}$. Setting this maximum equal to 1 and solving for F gives F = 1/2. Considering the denominator of equation (5), it is clear that, in general, solutions exist only for $\psi^2 < 1$. This places a constraint on the relation of F and $\hat{r}_o$. Figure 11 shows plots of the solution regimes for various contact angles. It can be seen that as the centrifugal force increases and F becomes more positive, the radius of intersection with the boundary increases. Physically, the fluid is being centrifuged away from the axis and the fluid intersects the boundary at a larger radius. As the rotation increases without limit the vapor core approaches a cylinder whose radius is governed by the vapor volume and L. The radius of intersection is particularly sensitive to F until F exceeds about one. Thus, when centrifugal forces dominate, the interface becomes more parallel with the rotation axis except at the boundaries where it must satisfy the contact angle constraint. As the contact angle increases, the intersection radius naturally increases. To summarize, for an isolated bubble, the shape of the bubble is determined solely by the parameter F. This parameter ranges from 0 for a spherical bubble to 1/2 for a cylindrical bubble. From the definition of F, it can be seen that for a constant F, a further increase in the rotation speed reduces the bubble radius which increases its length to conserve volume. Values of F greater than 1/2 can be permitted only if the top of the bubble breaks contact with the axis. Then permissible values of F are determined by the contact radius of the interface with the boundary.

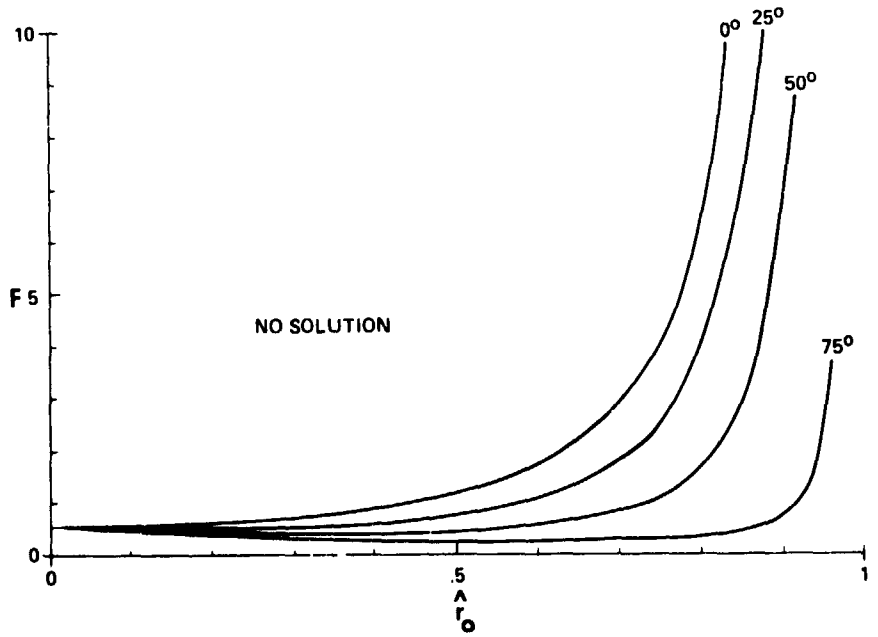

Figure 11. Solution regime of equation (5) for various contact angles.

DISCUSSION OF FLIGHT RESULTS

This section presents some of the free surface profiles from the flight experiments. Although many shapes were recorded, only a sample representing the extremes of F are presented here. Measurements of free surface shapes were compared with the model calculations for various values of F, $\hat{r}_o$, and L. For the calculations, the values of F and L as well as the vapor volumes were known from the experiment. The value of F was entered into equation (5). The value of $\hat{r}_o$ could not be easily determined from the overhead or side cameras particularly since θ is near zero. Instead, a guess of $\hat{r}_o$ was made and the equation was numerically integrated. If the computed value of z at $\hat{r} = \hat{r}_o$ was not equal to the known cylinder half-depth, a new guess for $\hat{r}_o$ was made. After the integration was complete, a check of the measured bubble volume with the computed volume was made.

Figures 12a, b, and c show a comparison of the measured interface profiles with the calculated ones for small, moderate, and large values of F, respectively. The cylinder depth is 2 cm. The profile in 12a is a low-rotation case which is dominated by capillary forces. These data were somewhat difficult

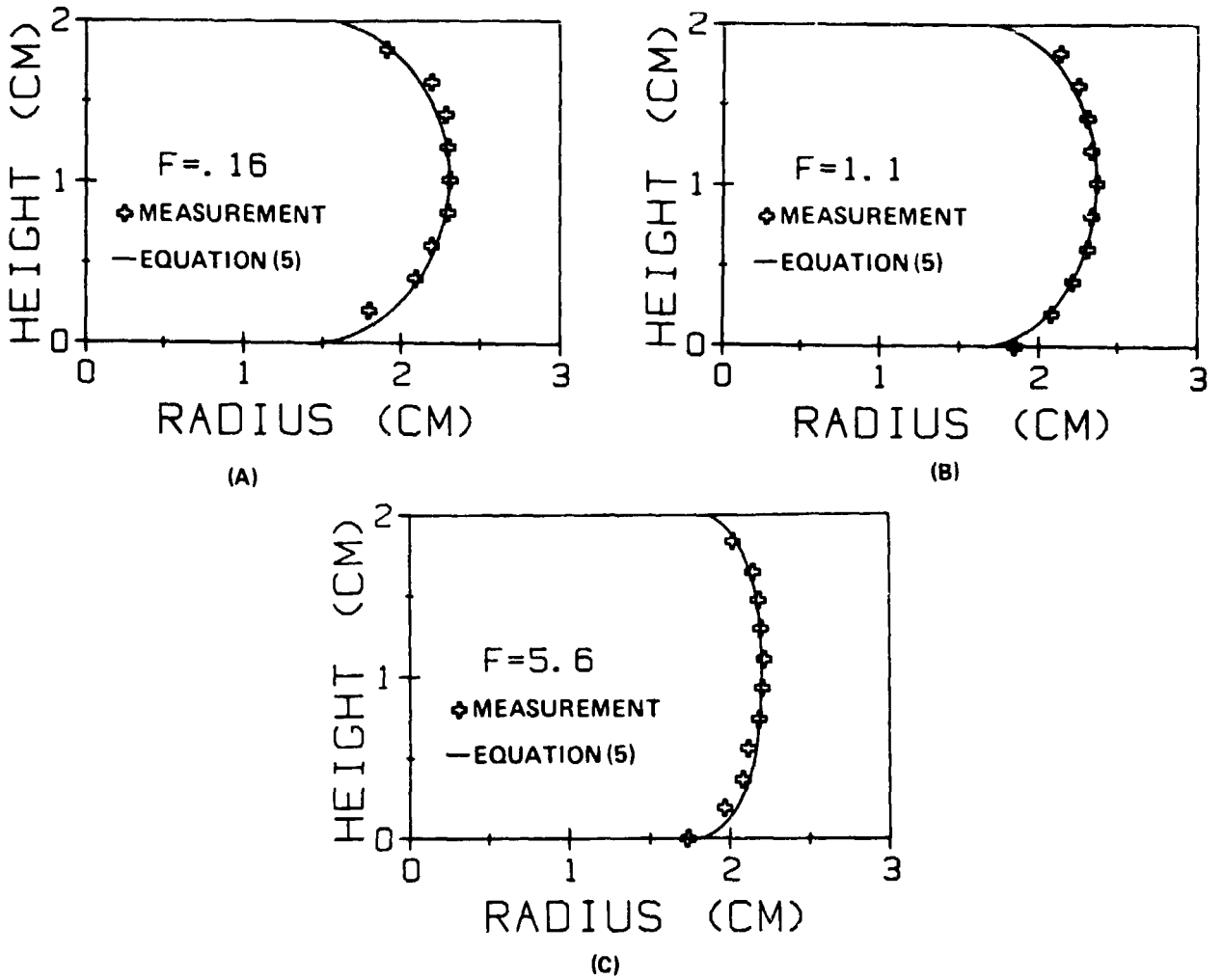

Figure 12. A comparison of the measured profile with the computed one in a 2 cm deep cylinder for (a) F = 0.16, (b) F = 1.1, and (c) F = 5.6.

to obtain because the equilibrium was very sensitive to the environment's departure from zero-gravity. Although the fluid behaved nearly quasi-steady as the environmental gravity diminished from 2-g's to near zero, establishment of a true equilibrium was transitory. Fluctuations around zero-gravity created vertical displacements of the bubble which sometimes broke contact with the top or bottom boundaries. Clearly for this case the interface surface is near spherical and is in good agreement with the calculations.

Figure 12b shows data for a moderate value of F. Here the capillary and centrifugal forces are about equal and the surface has become more prolate. It can be seen that the value of $\hat{r}_o$ has increased, consistent with Figure 11. Similarly, Figure 12c shows the data and calculated profiles for a large value of F. The surface here is dominated by centrifugal force and the interface is more parallel with the rotation axis, except at the boundary where it is constrained to intersect at a prescribed angle. For this value of F, the interface was quite stable because the centrifugal force was not only greater than the capillary force, but was also much greater than the fluctuating residual environmental gravity.

Figures 13a, b, and c show interface shapes for a cylinder depth of 4 cm. For a given bubble volume, larger rotation rates are needed in order for the bubble to contact the top and bottom boundaries as required by the theory. Otherwise, the bubble with a smaller diameter than the cylinder gap meanders along the axis or attaches to the top or bottom boundary. Figure 13a represents one of the slower relative rotation rates that could stabilize the bubble. Equation (5) can be used to determine the largest gap required to stabilize a bubble at a particular value of F. The tallest bubble that can be attained for a given F is found by using the smallest $\hat{r}_o$ that the solution will permit. Figure 14 shows computations of the interface shapes of isolated bubbles for various values of F. It is apparent that increasing the rotation increases the aspect ratio of the bubble. This occurs as F approaches its maximum value of 1/2 for an isolated bubble. A further increase of F after that point causes the bubble to break

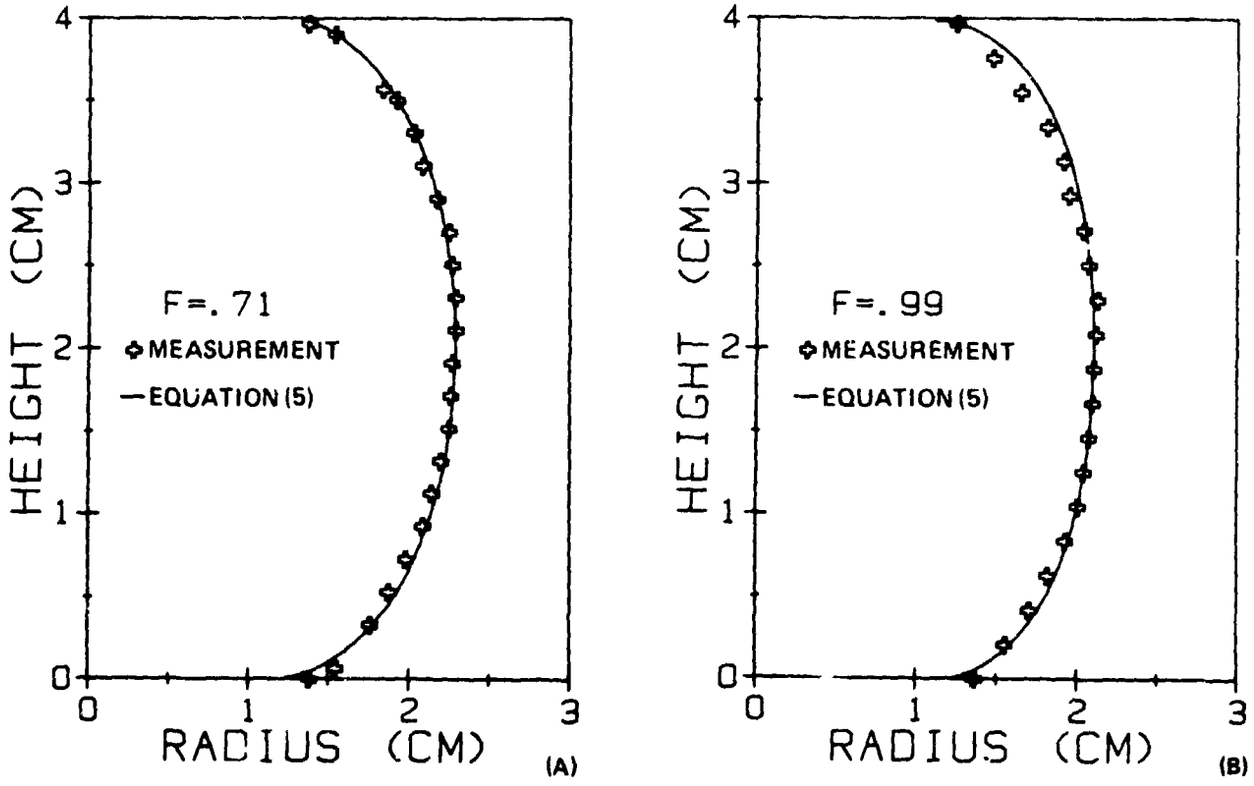

Figure 13. A comparison of the measured profile with the computed one in a 4 cm deep cylinder for (a) F = 0.71, (b) F = 0.99, and (c) F = 3.2.

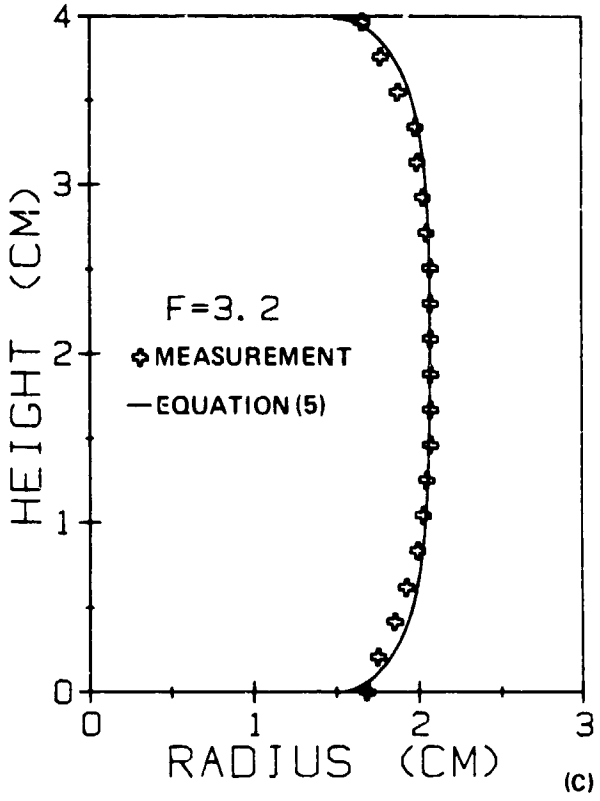

Figure 13. (Concluded).

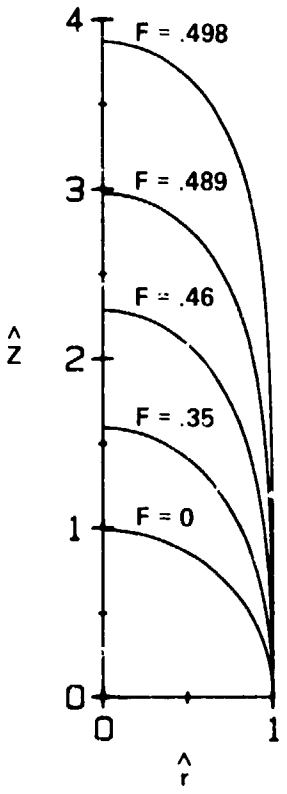

Figure 14. Computed interface shapes for isolated bubbles for various values of F.

contact with the axis of rotation and $\hat{r}_o$ becomes greater than 0. Once $\hat{r}_o$ increases, then the solution permits larger values of F consistent with Figure 11. Figure 13b shows a profile in which centrifugal and capillary forces are about equal. The value of F is about the same as for the profile in Figure 12b. However, $\hat{r}_o$ had to be appropriately decreased for the computation in order for the interface height to match the deeper container. Figure 13c shows an interface profile for F = 3. Because capillary forces are weak, the interface is almost cylindrical except for its contact point with the top and bottom boundaries. The capillary rise occurs over a thinner layer in order that the small radius of curvatuve can generate enough pressure drop to account for the increased hydrostatic contribution.

Finally, Figure 15 shows an interface profile for a rotating cylinder of 6.3 cm depth. For similar bubble volume to total volume ratios, higher values of F are required to produce an interface with top and bottom boundary contact. This simply means they require greater rotational speeds, since for these near-cylindrical bubbles the bubble radius changes little with ω. An increase in ω merely increases F producing a more cylindrical bubble. The figure shows the resulting thinner layer over which the surface tension acts to meet the contact angle requirement. This layer is thinner for the reason stated above.

Quantitative evaluation of the effects of baffles was difficult to accomplish aboard the KC-135 due to the g-fluctuations as well as the short duration of the low-gravity period. Some general remarks can be made however. The presence of the baffles clearly help to stabilize the interface by reducing the length scale of the problem. For cases where the cylinder depth was too great for the bubble to intersect both the top and bottom boundary (for a given rotation rate) the addition of baffles created smaller effective depths which tended to stabilize the bubbles. In other words, a baffled cylinder acted much like a series of independent shorter cylinders. An exception to this is for low rotation rates where the

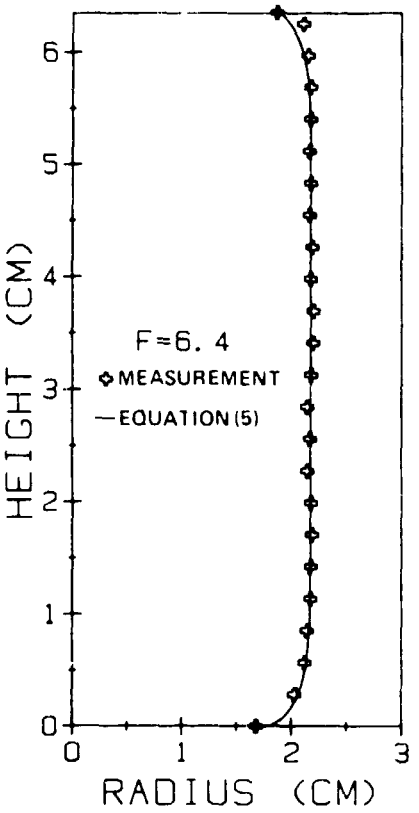

Figure 15. A comparison of the measured profile with the computed one in a 6.3 cm deep cylinder for F = 6.4.

type II instability becomes important. For these cases the theory predicts that the configuration will be unstable to small perturbations, although it does not predict what the final state will be. Figures 16 and 17 show photographs of single and double baffle configurations, respectively, in which the distribution of fluid in the different layers is clearly unequal. However, a similar configuration would occur with the addition of small, positive gravity. Comparison of the observations with the theory was difficult due to the fluctuations of the gravity environment. The stability boundary for this case could not be mapped out experimentally, but all of the configurations that were theoretically unstable were observed to be unstable. However, this was not the case for the configurations that were theoretically stable. Further verification of the nature of the type II instability will have to wait for results from experiments aboard an orbiting laboratory.

In summary, equation (5) derived from LaPlace's equation relating the pressure drop across an interface to the radii of curvature has been applied to a rotating bubble which contacts the container boundary. Solutions to the equation are dependent upon several parameters, viz F the ratio of centrifugal to capillary forces, $\hat{r}_o$ the contact radius of the interface to the boundary, and θ the contact angle. For the cases presented here the contact angle was near zero which permits a greater range of solutions. For isolated bubbles, F has a maximum value of 1/2. A further increase in F causes the bubble to break contact with the axis of rotation. For large values of F, the bubble becomes more cylindrical and the capillary rise occurs over a thinner layer. Measurements of the interface shapes performed in the low-gravity environment of an aircraft showed good agreement for the cases examined, indicating that equation (5) can be used to determine container baffle spacing required to confine a rotating bubble.

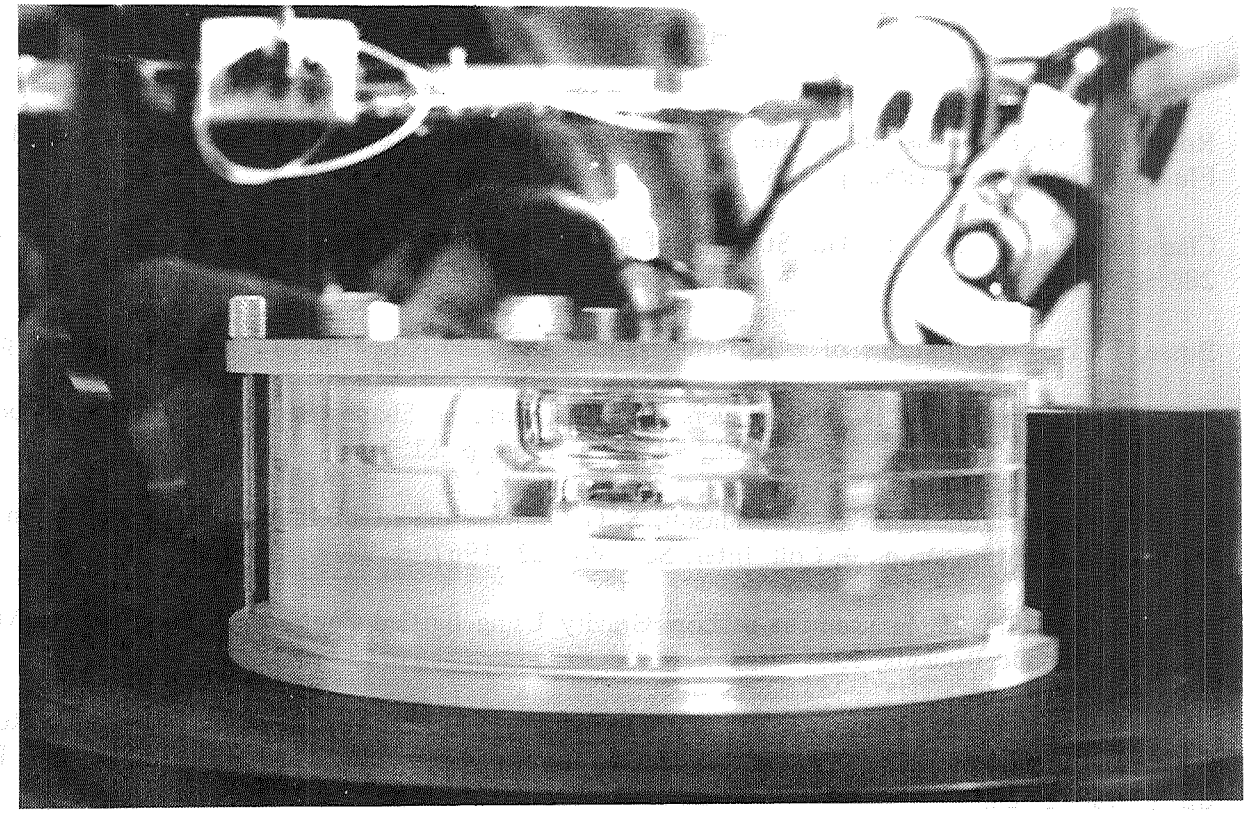

Figure 16. Photograph of a low gravity bubble in a rotating cylinder with one baffle.

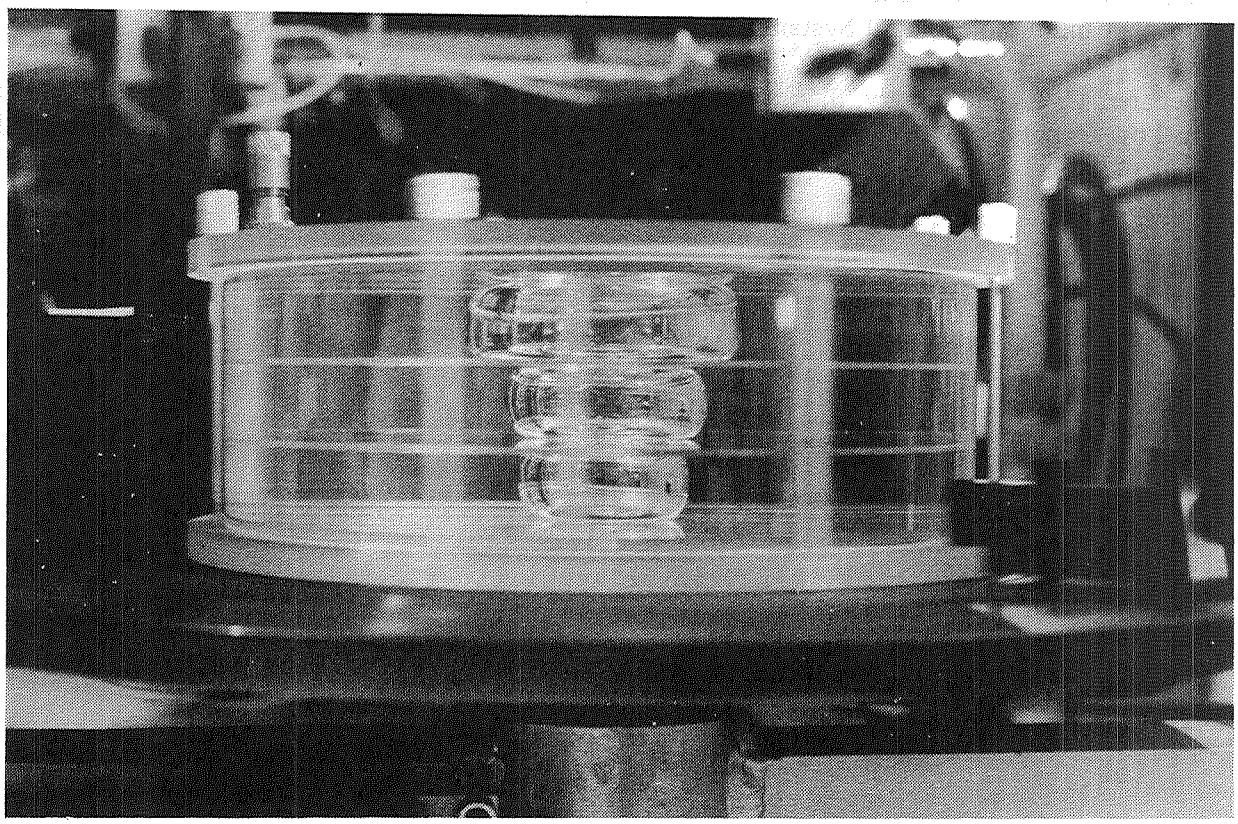

Figure 17. Photograph of a low gravity bubble in a rotating cylinder with two baffles.

REFERENCES

1. Rosenthal, D. K.: The Shape and Stability of a Bubble at the Axis of a Rotating Liquid. J. Fluid Mech., Vol. 12, 1962, p. 358.

2. Chandrasekhar, F. R. S.: The Stability of a Rotating Liquid Drop. Proc. R. Soc. Lond., Vol. 286, 1965, p. 1.

3. Busse, F. H.: Oscillations of a Rotating Liquid Drop. J. Fluid Mech., Vol. 142,, 1984, p. 1.

4. Tieu, H. A., Joseph, D. D., and Beavers, G. S.: Interfacial Shapes Between Two Superimposed Rotating Simple Fluids. J. Fluid Mech., Vol. 145, 1984, p. 11.

5. Princen, H. M., Zia, I. Y. Z., and Mason, S. G.: Measurement of Interfacial Tension from the Shape of a Rotating Drop. J. Coll. Inter. Sci., Vol. 23, 1967, p. 99.

6. Gans, R. F.: Liquid Management in Low Gravity Using Baffled Containers. To appear in AIAA J. Spacecraft and Rockets, 1985.

7. Wang, T. G., Tagg, R., Cammack, L., and Croonquist, A.: Non-Axisymmetric Shapes of a Rotating Drop in an Immiscible System. Proc. Sec. Internl. Colloquim Drop and Bubbles, JPL Pub. 82-7, 1982, p. 203.

8. Trinh, E., Zwern, A., and Wang, T. B.: An Experimental Study of Small-Amplitude Drop Oscillations in Immiscible Liquid Systems. J. Fluid Mech., Vol. 115, 1982, p. 453.

9. Schafer, C. F. and Lowry, S. A.: Mechanics of Liquid Helium in a Partially-Filled Rotating Dewar in Low Gravity – With Application to Gravity Probe-B. NASA Technical Paper 2124, January 1983.

1. REPORT NO.	2. GOVERNMENT ACCESSION NO.	3. RECIPIENT'S CATALOG NO.
NASA TP-2486		

4. TITLE AND SUBTITLE	5. REPORT DATE
Fluid Surface Behavior in Low Gravity Center Discretionary Fund No. 83-21, Final Report	June 1985 6. PERFORMING ORGANIZATION CODE
7. AUTHOR(S) Fred Leslie, Roger F. Gans, and Charles Schafer	8. PERFORMING ORGANIZATION REPORT #
9. PERFORMING ORGANIZATION NAME AND ADDRESS George C. Marshall Space Flight Center Marshall Space Flight Center, Alabama 35812	10. WORK UNIT NO. M-490 11. CONTRACT OR GRANT NO.
12. SPONSORING AGENCY NAME AND ADDRESS National Aeronautics and Space Administration Washington, D.C 20546	13. TYPE OF REPORT & PERIOD COVERED Technical Paper 14. SPONSORING AGENCY CODE

15. SUPPLEMENTARY NOTES

Prepared by Atmospheric Sciences Division, Systems Dynamics Laboratory.

16. ABSTRACT

Measurements of rotating equilibrium bubble shapes in the low-gravity environment of a free-falling aircraft are presented. Emphasis is placed on bubbles which intersect the container boundaries. These data are compared with theoretical profiles derived from Laplace's formula and are in good agreement with the measurements. Two types of instability are explored. The first occurs when the baffle spacing is too large for the bubble to intersect both the top and bottom boundaries. The second occurs when the hydrostatic pressure beneath a displaced free surface does not compensate for pressure change due to capillary forces. The interface shape depends on the contact angle, the radius of intersection with container, and the parameter F which is a measure of the relative importance of centrifugal force to surface tension. For isolated bubbles, F has a maximum value of 1/2. A further increase in F causes the bubble to break contact with the axis of rotation. For large values of F, the bubble becomes more cylindrical and the capillary rise occurs over a thinner layer so that the small radius of curvature can generate enough pressure drop to balance the increased hydrostatic contribution.

17. KEY WORDS	18. DISTRIBUTION STATEMENT
Low Gravity Fluid Mechanics Surface Tension Gravity Probe-B	Unclassified - Unlimited STAR Category 34

19. SECURITY CLASSIF. (of this report)	20. SECURITY CLASSIF. (of this page)	21. NO. OF PAGES	22. PRICE
Unclassified	Unclassified	27	A03

For sale by National Technical Information Service, Springfield, Virginia 22161
NASA-Langley 1985